

Article

An Acylhydrazone-Based Fluorescent Sensor for Sequential Recognition of Al^{3+} and H_2PO_4^-

Donghwan Choe  and Cheal Kim *

Department of Fine Chemistry, Seoul National University of Science and Technology (SNUT), Seoul 136-742, Korea; ehdghksdl_@naver.com

* Correspondence: chealkim@snut.ac.kr; Tel.: +82-2-972-6673; Fax: +82-2-981-9147

Abstract: A novel acylhydrazone-based fluorescent sensor **NATB** was designed and synthesized for consecutive sensing of Al^{3+} and H_2PO_4^- . **NATB** displayed fluorometric sensing to Al^{3+} and could sequentially detect H_2PO_4^- by fluorescence quenching. The limits of detection for Al^{3+} and H_2PO_4^- were determined to be 0.83 and 1.7 μM , respectively. The binding ratios of **NATB** to Al^{3+} and **NATB**- Al^{3+} to H_2PO_4^- were found to be 1:1. The sequential recognition of Al^{3+} and H_2PO_4^- by **NATB** could be repeated consecutively. In addition, the practicality of **NATB** was confirmed with the application of test strips. The sensing mechanisms of Al^{3+} and H_2PO_4^- by **NATB** were investigated through fluorescence and UV-Visible spectroscopy, Job plot, ESI-MS, ^1H NMR titration, and DFT calculations.

Keywords: aluminum ion; dihydrogen phosphate; acylhydrazone; fluorescent chemosensor; sequential detection; calculations



Citation: Choe, D.; Kim, C. An Acylhydrazone-Based Fluorescent Sensor for Sequential Recognition of Al^{3+} and H_2PO_4^- . *Materials* **2021**, *14*, 6392. <https://doi.org/10.3390/ma14216392>

Academic Editors: Marco Race, Elza Bontempi, Avelino Núñez-Delgado, Zhien Zhang, Mario Coccia and Yaoyu Zhou

Received: 23 September 2021
Accepted: 20 October 2021
Published: 25 October 2021

Publisher's Note: MDPI stays neutral with regard to jurisdictional claims in published maps and institutional affiliations.



Copyright: © 2021 by the authors. Licensee MDPI, Basel, Switzerland. This article is an open access article distributed under the terms and conditions of the Creative Commons Attribution (CC BY) license (<https://creativecommons.org/licenses/by/4.0/>).

1. Introduction

Al^{3+} , the third most abundant metallic element in nature [1,2], is broadly employed in daily life in packaging materials, pharmaceuticals, food additives, machinery, clinical medicines, and water purification [3,4]. Owing to its widespread usage, Al^{3+} could be readily accumulated in the body, which leads to the development of diverse diseases such as Parkinson's and Alzheimer's disease [5,6]. Dihydrogen phosphate (H_2PO_4^-) is an important component related to many intercellular activities, such as signaling mediation, protein phosphorylation, enzymatic reactions, ion-channel regulation, and so on [7–9]. However, excessive agricultural use of phosphate causes eutrophication or massive algal growth, leading to a deficiency in oxygen levels [10–12]. For these reasons, there has been a strong demand for the development of sensing and detection methods for Al^{3+} and H_2PO_4^- .

The traditional analytical methods reported for the analysis of cations and anions, such as ICP-AES, AAS, and electrochemical methods, have been largely restricted due to their expensive instruments, complicated procedures, and the need for highly trained operators [13–15]. In contrast, fluorescence methods have shown the advantages of cost-effectiveness, simplicity, easy operation, and high sensitivity [16–18]. While numerous fluorescent chemosensors for a single analyte have been reported, fluorescent chemosensors that allow the sequential sensing of multiple analytes with great selectivity and sensitivity are still needed [19–21] because they are more cost-effective, recyclable and practical [22–24]. Several fluorescent sensors have been addressed for consecutive sensing of Al^{3+} and several anions [25–28] or several cations and H_2PO_4^- [29–31]. In addition, Kumar et al. reported a fluorescent sensor for sequential sensing of Al^{3+} and $\text{H}_2\text{PO}_4^-/\text{HSO}_4^-$ [32]. The practical importance of sequential sensing may have potential applications such as logic gates and molecular switches. Nevertheless, a sequential fluorescent sensor that can exclusively detect Al^{3+} and H_2PO_4^- has not been reported to date.

As Al^{3+} is a hard cation, chemosensors containing hard base units, such as nitrogen or oxygen atoms, prefer to coordinate with Al^{3+} [33–35]. In this regard, acylhydrazone derivatives, having oxygen and nitrogen atoms, are expected to be a suitable functional group to design an Al^{3+} chemosensor [36–38]. Naphthalene moieties have been widely applied for the design of fluorescent sensors because of their excellent photophysical properties as a fluorophore [39–41]. Hence, we expected that a compound including both acylhydrazone and naphthalene may operate as a fluorescence chemosensor for Al^{3+} .

In the current study, we designed an acylhydrazone-based fluorescent sensor, **NATB**, which showed green fluorescence emissions with Al^{3+} and could sequentially detect H_2PO_4^- through fluorescence quenching with high sensitivity and selectivity. A sensing mechanism of **NATB** to Al^{3+} and H_2PO_4^- was illustrated by fluorescence and UV–Vis spectroscopy, Job plot, ESI-MS, ^1H NMR titration, and calculations.

2. Experimental Section

2.1. Materials and Equipment

All solvents and reagents were commercially obtained from TCI (TCI, Nihonbashi-Honcho, Tokyo, Japan) and Sigma-Aldrich (MilliporeSigma, Burlington, MA, USA). NMR experiments were conducted using $\text{DMSO}-d_6$ as the solvent, and the data were recorded on a Varian spectrometer (Varian, Palo Alto, CA, USA). Fluorescence and UV–Visible spectra were measured with Perkin Elmer machines (Perkin Elmer, Waltham, MA, USA). The quantum yields of **NATB** and **NATB**- Al^{3+} were relatively determined with quinine ($\Phi = 0.54$ in 1×10^{-1} M H_2SO_4) as a reference. ESI-MS data were recorded on a Thermo Finnigan machine (Thermo Finnigan LLC, San Jose, CA, USA).

2.2. Synthesis of *N'*-(*E*)-(3-*tert*-butyl-2-hydroxyphenyl)methylidene]-3-hydroxynaphthalene-2-carbohydrazide (**NATB**)

The intermediate compound, 3-hydroxy-2-naphthohydrazide (**2**), was synthesized following a previously reported method [42]. The excess amounts of 3-(*tert*-butyl)-2-hydroxybenzaldehyde (**1**, 1.8 mmol) and 3-hydroxy-2-naphthohydrazide (**2**, 0.3 mmol) were mixed in absolute EtOH (10 mL) with a catalytic amount of HCl and stirred at room temperature for 1 day. A yellow precipitate was filtered, rinsed with cold absolute EtOH, and dried (77.2 mg, 70.1%); ^1H NMR in $\text{DMSO}-d_6$: δ 12.42 (s, 1H), 12.24 (s, 1H), 11.19 (s, 1H), 8.63 (s, 1H), 8.45 (s, 1H), 7.93 (d, 1H), 7.77 (d, 1H), 7.53 (t, 1H), 7.38 (t, 1H), 7.35 (s, 1H), 7.32 (d, 1H), 7.30 (d, 1H), 6.91 (t, 1H), 1.43 (s, 9H). ^{13}C NMR in $\text{DMSO}-d_6$: δ 163.23 (1C), 156.90 (1C), 153.75 (1C), 151.45 (1C), 136.36 (1C), 135.84 (1C), 130.31 (1C), 129.53 (1C), 128.59 (1C), 128.54 (1C), 128.20 (1C), 126.69 (1C), 125.75 (1C), 123.75 (1C), 119.86 (1C), 118.70 (1C), 117.54 (1C), 110.54 (1C), 34.39 (1C), 29.16 (3C). ESI-MS (*m/z*): [**NATB** + H^+] $^+$ calcd 363.17, found 363.04.

2.3. Preparation of Spectroscopic Experiments

An **NATB** stock (10 mM) was prepared in DMSO. The stock solutions (20 mM) of varied cations were prepared using their nitrate salts (Al^{3+} , Na^+ , Cr^{3+} , Fe^{2+} , Ca^{2+} , Cd^{2+} , Zn^{2+} , Pb^{2+} , Co^{2+} , Cu^{2+} , In^{3+} , Mn^{2+} , Ga^{3+} , Ni^{2+} , Mg^{2+} , Ag^+ , Hg^{2+} and K^+) or perchlorate salt (Fe^{3+}). The concentrated solutions (20 mM) of varied anions were prepared using their tetrabutylammonium salts (H_2PO_4^- , SCN^- , BzO^- , N_3^- , OAc^- and NO_2^-), tetraethylammonium salts (F^- , Cl^- , Br^- , I^- and CN^-), sodium salts (S^{2-} and ClO^-), or potassium salts (HPO_4^{2-} , PO_4^{3-} , HSO_4^- and $\text{P}_2\text{O}_7^{4-}$ (PPi)). All spectroscopic experiments were conducted in MeOH.

2.4. Competitive Experiments

For Al^{3+} , 6 μL (10 mM) of an **NATB** stock in DMSO was mixed into MeOH (2 mL) to make 30 μM . A total of 4.5 μL of various cations (20 mM) in DMF was diluted in **NATB** to make 45 μM . Finally, 4.5 μL (20 mM) of an Al^{3+} stock in DMF was mixed into each solution to produce 45 μM , and their fluorescent spectra were measured.

For H_2PO_4^- , 6 μL (10 mM) of an **NATB** stock in DMSO and 4.5 μL (20 mM) of an Al^{3+} stock in DMF were diluted into MeOH (2 mL) to produce 30 μM of **NATB**- Al^{3+} . We added 4.5 μL of various anions (20 mM) in H_2O to **NATB**- Al^{3+} to produce 45 μM . A total of 4.5 μL (20 mM) of an H_2PO_4^- stock was diluted into each solution to produce 45 μM . Their fluorescent spectra were measured.

2.5. Determination of Association Constant (*K*)

The association constant (*K*) was calculated using Li's method [43]. If the ligand (*L*) and the analyte (*M*) form an m-n complex, M_mL_n , the equilibrium constant of the corresponding complex, *K*, can be expressed by the following equation:

$$[M]^m = \frac{1}{nK} \frac{1}{[L]_T^{n-1}} \frac{1-\alpha}{\alpha^n}$$

where,

$[M]$ = the concentration of analyte

$[L]_T$ = the total concentration of ligand

and α could be described as:

$$\alpha = \frac{I - I_{max}}{I_{min} - I_{max}}$$

where,

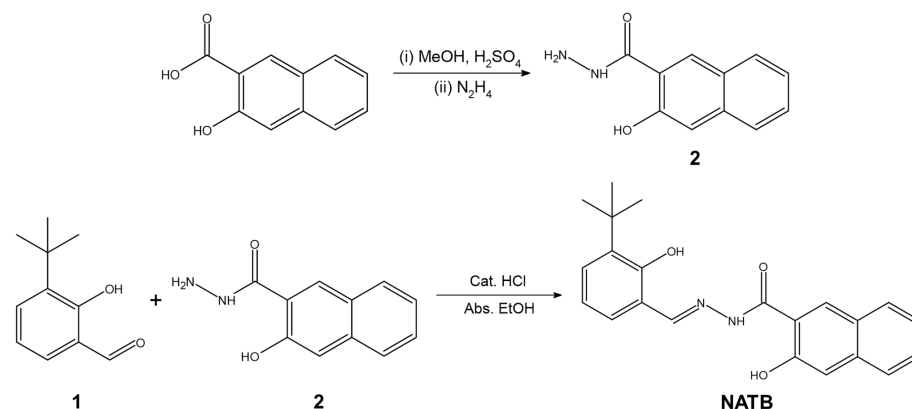
I = the fluorescence intensity of complex

2.6. Calculations

Calculations were achieved with the Gaussian 16 program [44]. Optimal geometries of **NATB** and **NATB**- Al^{3+} were provided with the DFT method [45,46]. B3LYP was selected as the hybrid functional basis set. The 6-31G(d,p) basis set was implemented to all atoms except Al^{3+} [47,48], and the LANL2DZ basis set was employed for applying ECP to Al^{3+} [49–51]. No imaginary frequency was found in the optimized states of **NATB** or **NATB**- Al^{3+} , indicating their local minima. The solvent effect of MeOH was considered with IEFPCM [52]. Based on the energy-optimized structures of **NATB** and **NATB**- Al^{3+} , the plausible UV-Vis transition states were calculated by the TD-DFT method with 20 lowest singlet states.

3. Results and Discussion

The synthesis of **NATB** was conducted as depicted in Scheme 1. The condensation reaction of 3-(*tert*-butyl)-2-hydroxybenzaldehyde (**1**) and 3-hydroxy-2-naphthohydrazide (**2**) produced the desired product, *N'*-(*E*)-(3-*tert*-butyl-2-hydroxyphenyl)methylidene]-3-hydroxynaphthalene-2-carbohydrazide (**NATB**), which was verified with ^1H NMR, ^{13}C NMR (Figures S1 and S2), and ESI-MS.



Scheme 1. Synthesis of **NATB**.

3.1. Spectroscopic Examination of NATB to Al³⁺

To confirm the fluorescence selectivity of **NATB**, the fluorescence emission was studied with a variety of cations in MeOH (Figure 1). As a result, **NATB** exhibited notable fluorescence emission at 526 nm with Al³⁺, while **NATB** and **NATB** with other cations showed negligible or no fluorescence emission ($\lambda_{\text{ex}} = 358 \text{ nm}$). These outcomes demonstrated that **NATB** could be utilized as a fluorescent probe for the selective sensing of Al³⁺. On the other hand, **NATB** was soluble in aqueous media, but it did not show any selectivity to Al³⁺. In addition, the fluorescence emission of **NATB** was examined with various anions including dihydrogen phosphate. **NATB** had no selectivity for the anions.

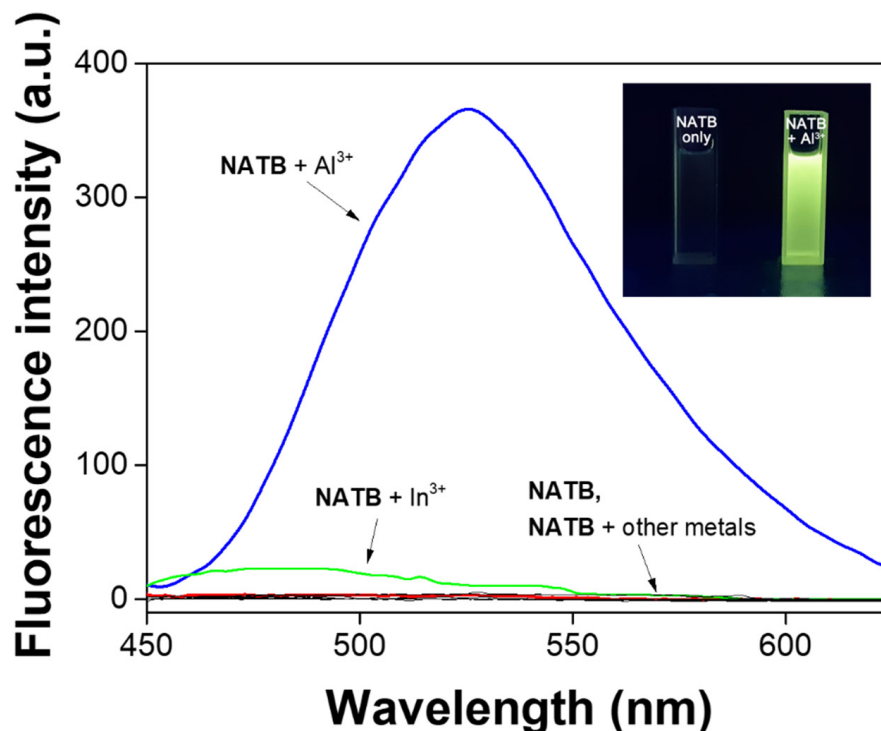


Figure 1. Fluorescence changes of **NATB** (30 μM) with a variety of cations (1.5 equiv) in MeOH. Photograph: the fluorescent images of **NATB** and **NATB**-Al³⁺ (λ_{ex} : 358 nm).

To check the concentration-dependent properties of **NATB** to Al³⁺, fluorescence titration was carried out (Figure 2). **NATB** exhibited little fluorescence with a tiny quantum yield ($\Phi = 0.008$). However, the continuous increase in Al³⁺ up to 1.5 equiv significantly enhanced the green fluorescence emission at 526 nm ($\Phi = 0.162$). UV-Vis spectrometry was also conducted with Al³⁺ to examine its photophysical characteristics (Figure 3). Upon the addition of Al³⁺, the absorption of 310 nm clearly decreased, while a new absorption of 325 nm constantly increased up to 1.5 equiv. An explicit isosbestic point was observed at 315 nm, verifying that the coordination of **NATB** with Al³⁺ produced a stable complex.

A 1:1 stoichiometric coordination between **NATB** and Al³⁺ was suggested by the Job plot experiment (Figure S3), which was explicitly supported by ESI-MS analysis (Figure S4). The positive ion mass displayed a large peak of 596.16 (m/z), which was correlated to $[\text{NATB}(-\text{H}^+) + \text{Al}^{3+} + 2 \text{DMF} + \text{NO}_3^-]^+$ (calcd. 596.23). The association constant (K) of **NATB**-Al³⁺ was confirmed to be $3.6 \times 10^4 \text{ M}^{-1}$ (Figure S5) based on Li's method [43]. The detection limit of **NATB** toward Al³⁺ was 0.83 μM , based on $3\sigma/\text{slope}$ (Figure S6).

The ¹H NMR titrations were achieved to investigate the binding mechanism of **NATB** toward Al³⁺ (Figure 4). Upon the addition of Al³⁺ to **NATB**, the proton H₁₄ continually disappeared and the protons H₅ and H₆ were deshielded. These results indicate that the deprotonated oxygen on the *tert*-butylphenol group and the oxygen and nitrogen on the acylhydrazone group may be coordinated to Al³⁺ (Scheme 2).

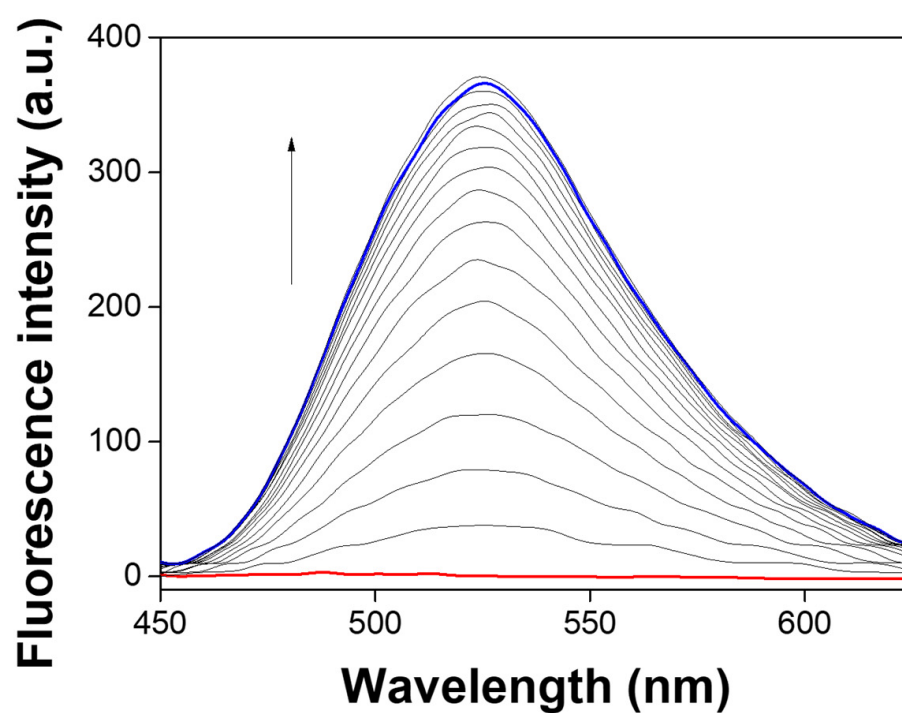


Figure 2. Fluorescence titration of NATB (30 μM) with varied amounts of Al^{3+} (0–1.5 equiv) in MeOH.

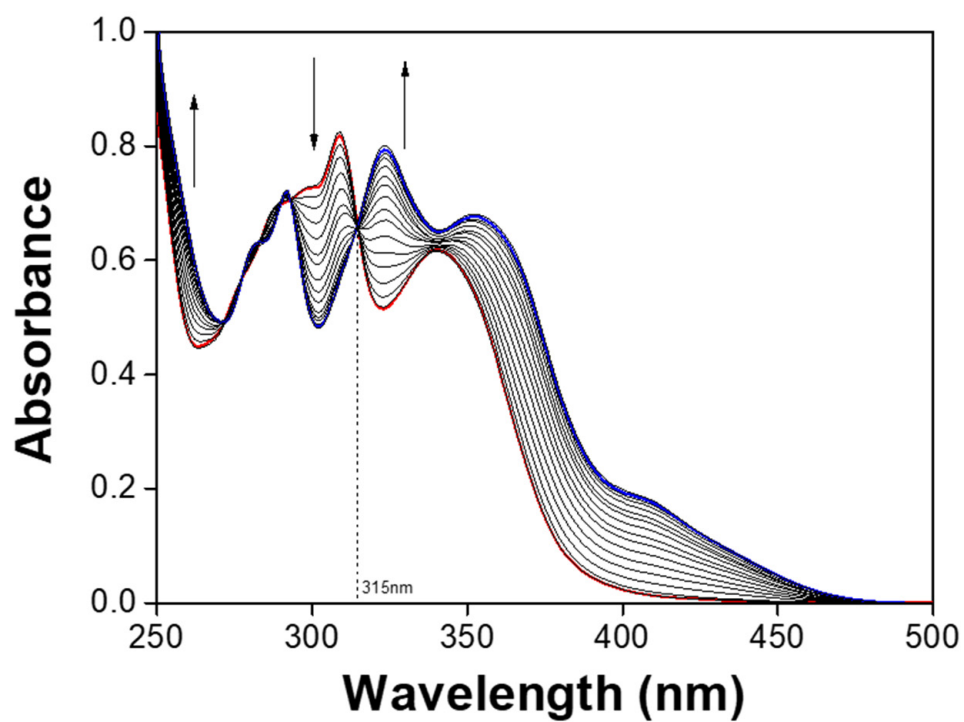


Figure 3. UV-Vis changes of NATB (30 μM) with varied amounts of Al^{3+} (0–1.5 equiv) in MeOH.

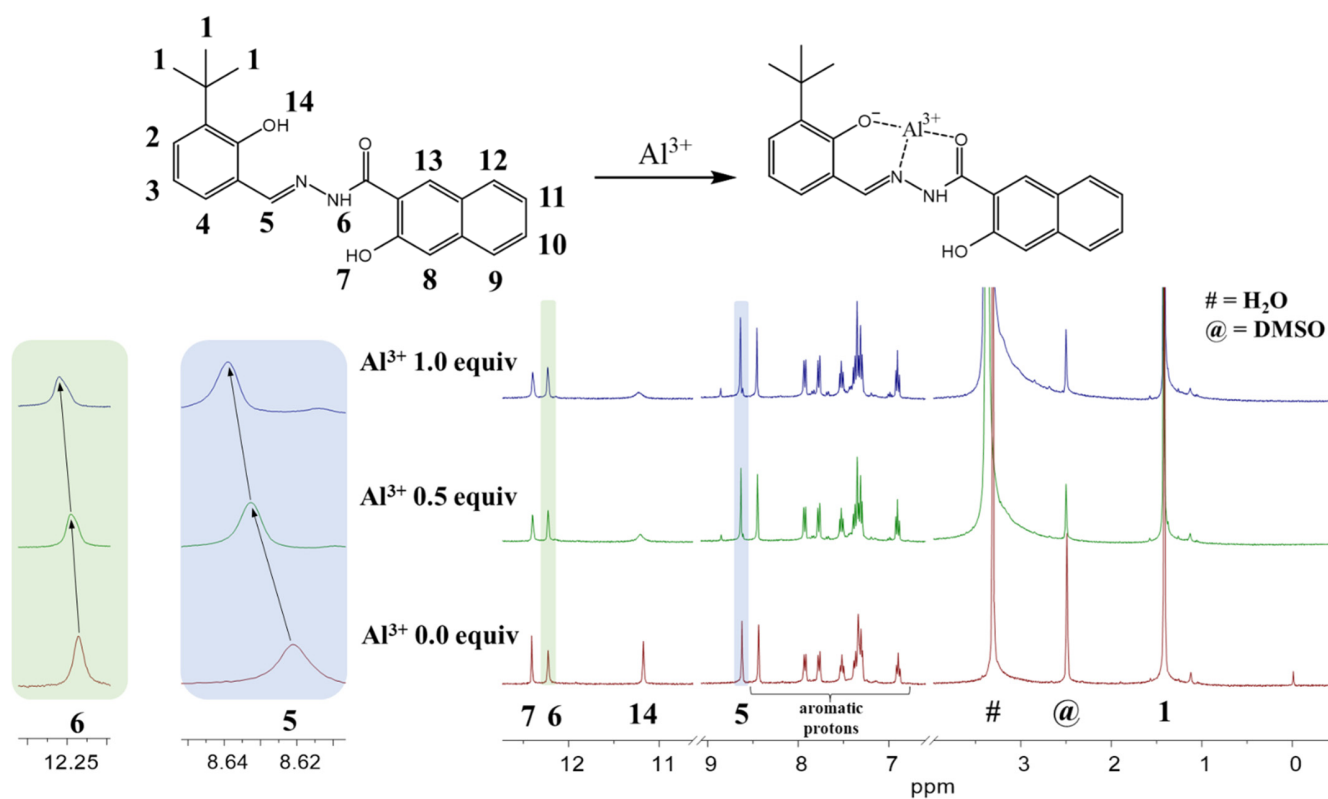
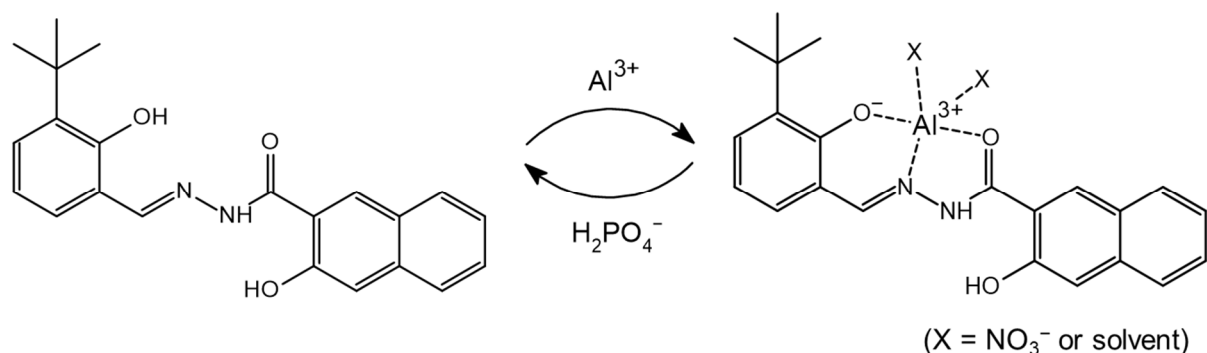


Figure 4. ^1H NMR titration of NATB with Al^{3+} in $\text{DMSO-}d_6$.



Scheme 2. Sequential recognition mechanism of Al^{3+} and H_2PO_4^- by NATB.

To verify the practicability of NATB as a probe for Al^{3+} , an interference experiment was conducted (Figure S7). NATB could detect Al^{3+} with other cations without significant interferences, except for In^{3+} , Fe^{3+} and Cu^{2+} . These three cations bound more tightly to NATB than Al^{3+} . For the practical application of NATB, test kits were prepared by immersing filter paper strips in the NATB solution. When NATB-coated test kits were immersed in a range of concentrations of Al^{3+} solutions, the obvious green fluorescence emission showed up above 2 mM of Al^{3+} under UV light (Figure 5a). However, the fluorescence was not displayed when those strips were applied to the same concentration of other cations (Figure 5b). These results indicate the potential applications of NATB in easily recognizing Al^{3+} without any complicated tools.

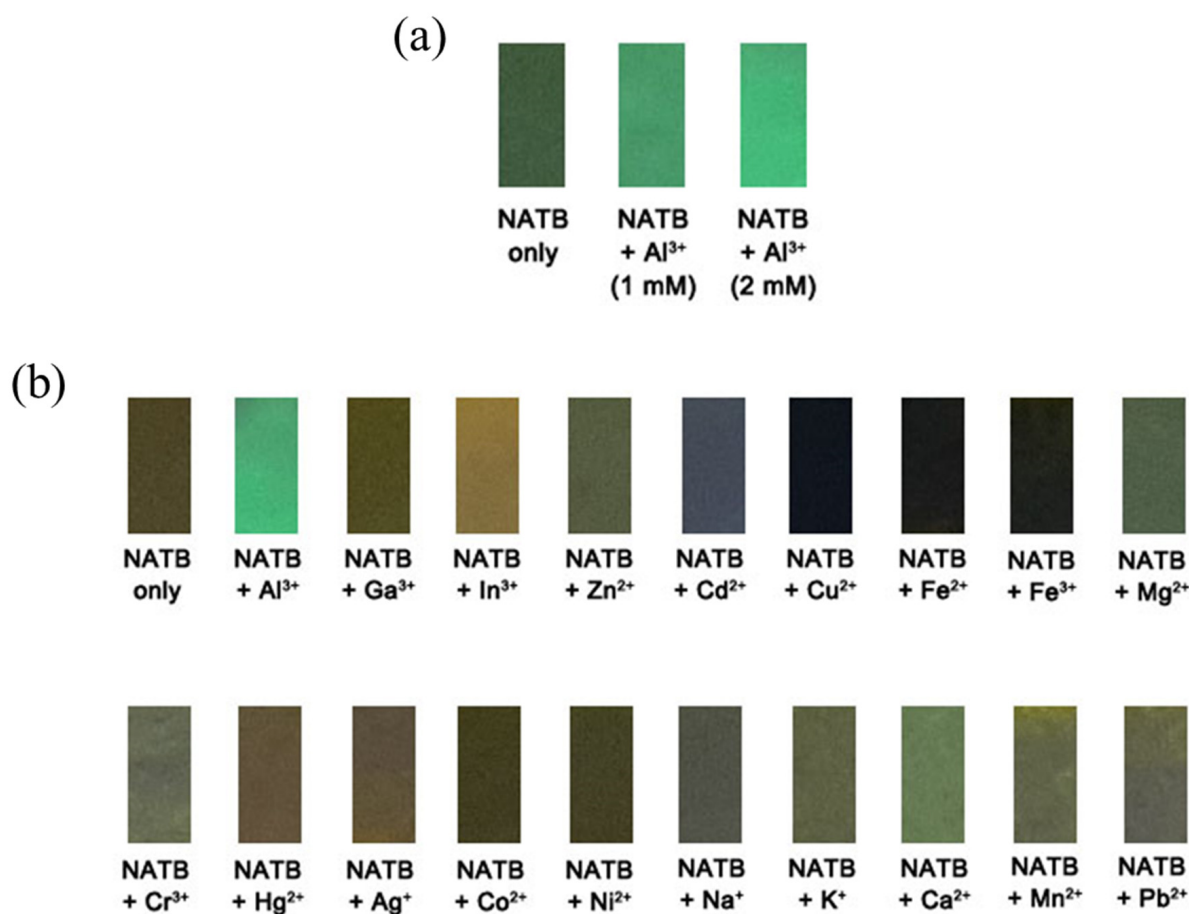


Figure 5. Detection of Al³⁺ by NATB-coated test kits (10 mM). (a) NATB-coated test kits immersed in the solution of different Al³⁺ concentrations; (b) NATB-coated test kits immersed in 2 mM of various cation solutions.

3.2. Calculations

To comprehend the Al³⁺-sensing property of NATB, DFT calculations were performed with the Gaussian 16 program (Figure 6). As the Job plot, ESI-MS, and ¹H NMR titration implied a 1:1 stoichiometric coordination of NATB with Al³⁺, all calculations were conducted with 1:1 stoichiometry. NATB showed a dihedral angle of 0.013° (1O, 2C, 3N, and 4C) with a planar structure (Figure 6a). The coordination of NATB with Al³⁺ distorted its structure, showing a dihedral angle of 98.875° (Figure 6b).

Based on the energy-minimized structures of NATB and NATB-Al³⁺, TD-DFT calculations were conducted to inspect the transition energies and molecular orbitals. NATB featured the main absorption induced from the HOMO → LUMO (347.28 nm), showing intra-charge transfer (ICT) transition from the *tert*-butylphenol to the naphthol (Figure S8). The major absorption of NATB-Al³⁺ derived from the HOMO-1 → LUMO transition (412.27 nm) also showed a similar ICT transition (Figures S9 and S10). The reduction in the energy gap was consistent with the red-shift of the experimental absorption. These outcomes led us to conclude that the fluorescence turn-on mechanism of NATB to Al³⁺ may be a chelation-enhanced fluorescence (CHEF) effect [53]. Based on experimental data and theoretical calculations, an appropriate binding structure of NATB-Al³⁺ is proposed in Scheme 2.

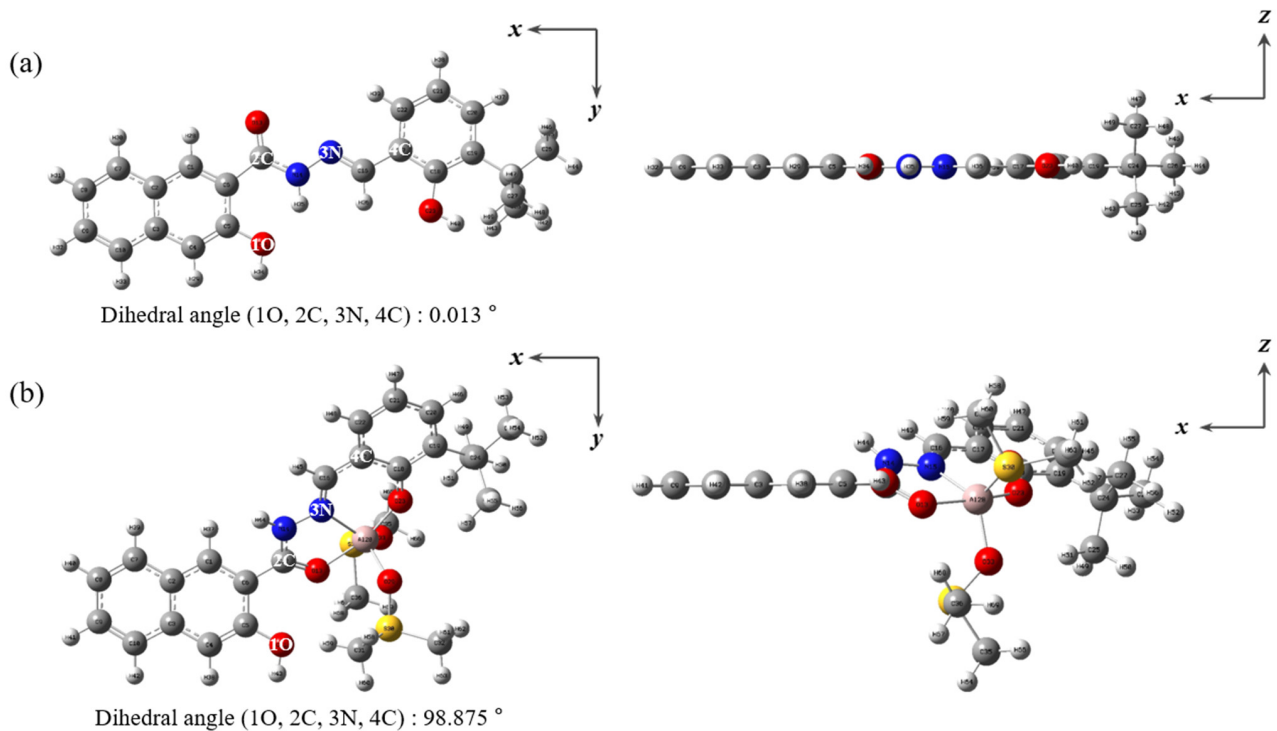


Figure 6. Energy-optimized forms of (a) NATB and (b) NATB-Al³⁺.

3.3. Spectroscopic Examination of NATB-Al³⁺ to H₂PO₄[−]

We studied the fluorescence selectivity of NATB-Al³⁺ to a range of anions such as H₂PO₄[−], Cl[−], CN[−], OAc[−], F[−], ClO[−], I[−], N₃[−], BzO[−], SCN[−], Br[−], NO₂[−], S^{2−}, HPO₄^{2−}, PO₄^{3−}, HSO₄[−], and PPI in MeOH (Figure 7). Most of the anions did not affect the fluorescence emission of NATB-Al³⁺, while the addition of H₂PO₄[−] toward NATB-Al³⁺ resulted in significant fluorescence quenching ($\lambda_{\text{ex}} = 358 \text{ nm}$). The result demonstrated that NATB-Al³⁺ could be used as a chemosensor for H₂PO₄[−] with fluorescence quenching.

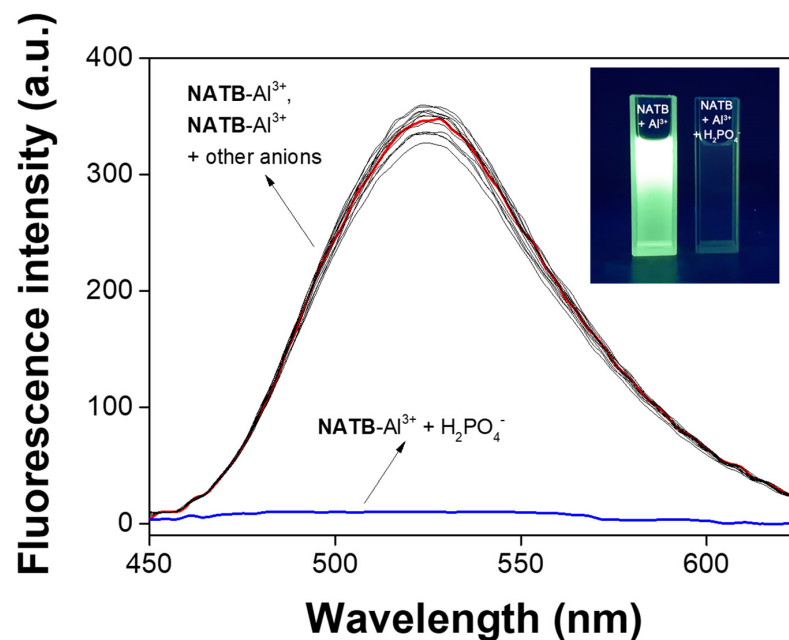


Figure 7. Fluorescence changes of NATB-Al³⁺ (30 μM) with various anions (45 μM) in MeOH (λ_{ex} : 358 nm). Photograph: the fluorescent images of NATB-Al³⁺ and NATB-Al³⁺-H₂PO₄[−] (λ_{ex} : 358 nm).

The fluorescence titration experiments were conducted to verify the fluorescence quenching ability of H_2PO_4^- toward NATB-Al^{3+} (Figure 8). The fluorescence of NATB-Al^{3+} consistently diminished with the addition of H_2PO_4^- up to 1.5 equiv ($\Phi = 0.005$). UV-Vis spectroscopy showed that the continuous addition of H_2PO_4^- increased the absorbance at 310 nm, while those at 270 and 325 nm decreased with the explicit isosbestic points at 253 and 315 nm (Figure 9). The UV-Vis spectrum of H_2PO_4^- with NATB-Al^{3+} is analogous to that of free NATB , implying that the addition of H_2PO_4^- released Al^{3+} from the NATB-Al^{3+} complex (Figure S11).

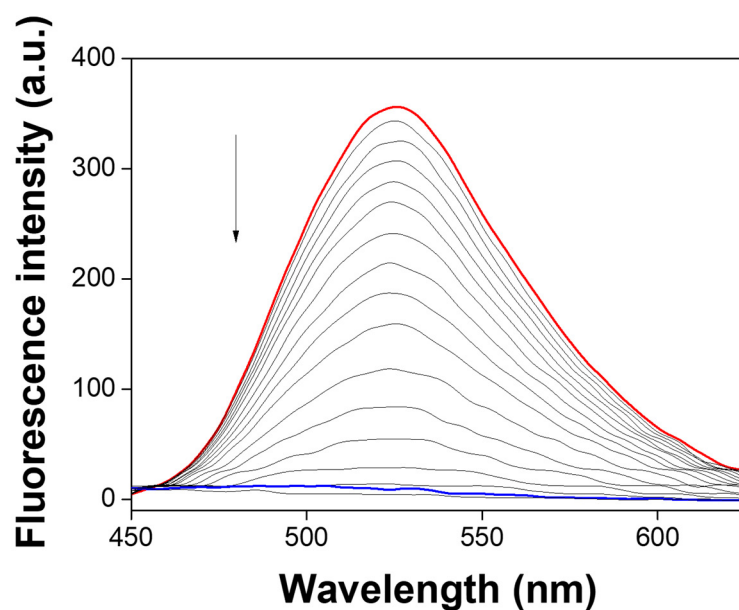


Figure 8. Fluorescence titration of NATB-Al^{3+} ($30 \mu\text{M}$) with various amounts of H_2PO_4^- (0–1.5 equiv) in MeOH.

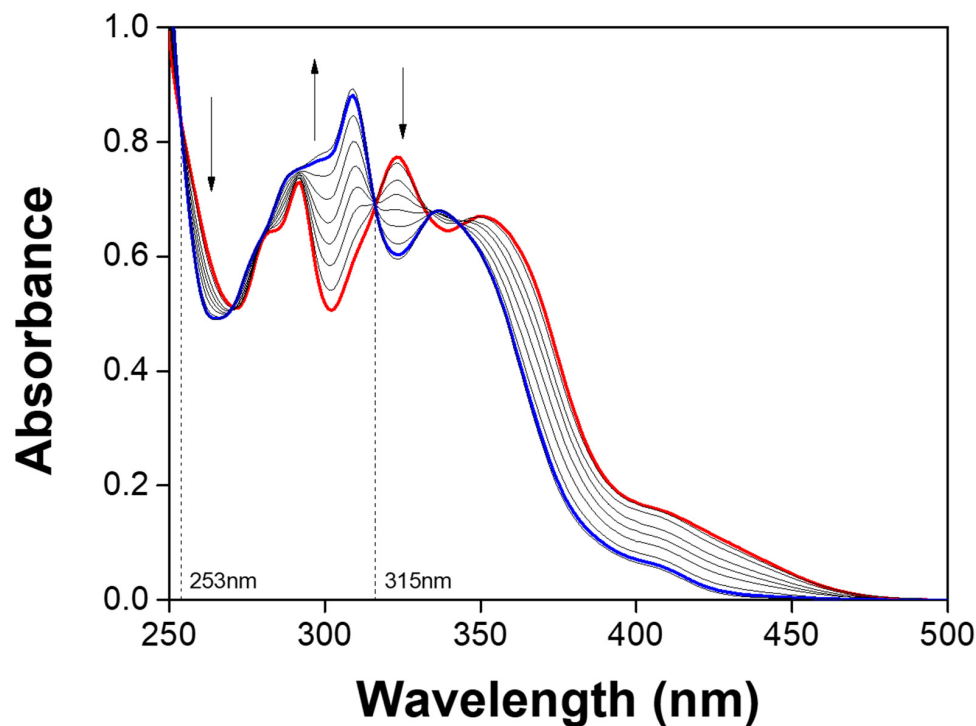


Figure 9. UV-Vis changes of NATB-Al^{3+} ($30 \mu\text{M}$) with various amounts of H_2PO_4^- (0–1.5 equiv) in MeOH.

The stoichiometry of H_2PO_4^- toward NATB-Al^{3+} was determined by the Job plot experiment (Figure S12), which exhibited a 1:1 stoichiometry. The mass spectral analysis displayed a peak of 395.06 (m/z), which demonstrated the regeneration of **NATB** ($[\text{NATB} + \text{H}^+ + \text{MeOH}]^+$; calcd. 395.20) (Figure S13). These outcomes supported the mechanism that the addition of H_2PO_4^- released Al^{3+} from NATB-Al^{3+} , which resulted in the loss of fluorescence. Based on Li's method [43], the association constant (K) for H_2PO_4^- with NATB-Al^{3+} was calculated as $1.2 \times 10^4 \text{ M}^{-1}$ (Figure S14). The detection limit of NATB-Al^{3+} toward H_2PO_4^- was determined as $1.7 \mu\text{M}$, based on $3\sigma/\text{slope}$ (Figure S15). Importantly, **NATB** is the first fluorescent sensor for the consecutive sensing of Al^{3+} and H_2PO_4^- (Table S1). On the other hand, **NATB** showed higher detection limits for Al^{3+} and H_2PO_4^- compared to Kumar's work [32], but it could solely detect H_2PO_4^- without the interference of HSO_4^- .

The reversibility in the response of **NATB** was verified through the alternative additions of Al^{3+} and H_2PO_4^- (Figure 10). The fluorescence emission of **NATB** repeated its enhancing and quenching processes several times without fluorescence efficiency loss. To verify that NATB-Al^{3+} is an effective fluorescence probe for H_2PO_4^- , the interference of other anions was tested (Figure S16). The results indicated that the presence of other anions (1.5 equiv) did not interfere with the fluorescence quenching of NATB-Al^{3+} toward H_2PO_4^- .

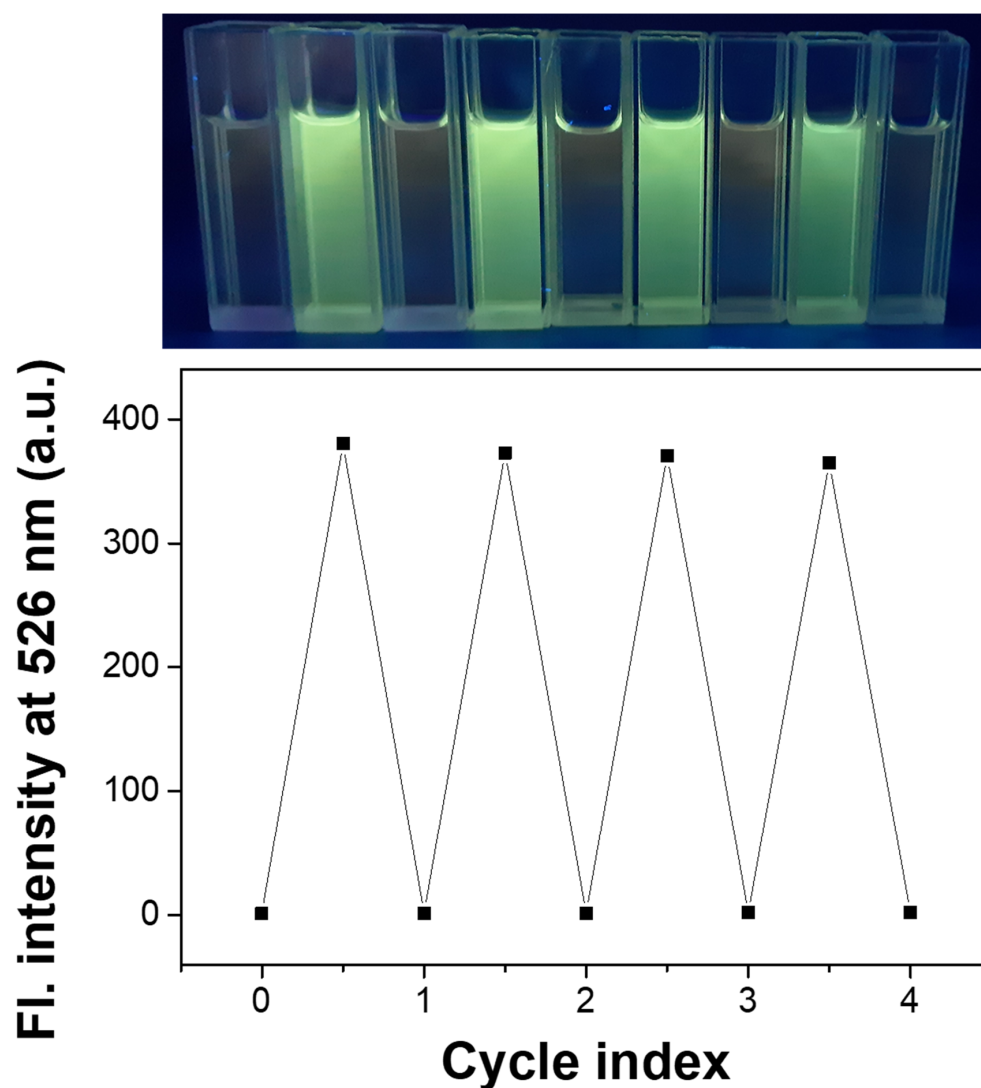


Figure 10. Change in fluorescence of **NATB** ($30 \mu\text{M}$) upon alternate addition of Al^{3+} and H_2PO_4^- in MeOH (λ_{ex} : 358 nm).

4. Conclusions

An acylhydrazone-based chemosensor **NATB** was developed and its sequential recognition of Al^{3+} and H_2PO_4^- was studied. **NATB** showed a strong fluorescence increase with Al^{3+} , and its complex **NATB**- Al^{3+} sequentially detected H_2PO_4^- by releasing Al^{3+} with turn-off fluorescence. Importantly, **NATB** is the first sequential fluorescent probe for selective sensing of Al^{3+} and H_2PO_4^- . Detection limits of **NATB** for Al^{3+} and H_2PO_4^- were calculated as 0.83 and 1.7 μM , respectively, based on $3\sigma/\text{slope}$. **NATB** could repeat sequential recognition of Al^{3+} and H_2PO_4^- several times and could be applied to detect Al^{3+} in test strips. The sensing mechanism of **NATB** toward Al^{3+} and H_2PO_4^- was demonstrated with a Job plot, ESI-MS, ^1H NMR spectroscopy, and theoretical calculations. The detection mechanism of **NATB** toward Al^{3+} is suggested to be a CHEF effect through DFT calculations.

Supplementary Materials: The following are available online at <https://www.mdpi.com/article/10.3390/ma14216392/s1>, Table S1: Examples of chemosensors for successive detection related to Al^{3+} or H_2PO_4^- or both; Figure S1: ^1H NMR spectrum of **NATB** in $\text{DMSO}-d_6$; Figure S2: ^{13}C NMR spectrum of **NATB** in $\text{DMSO}-d_6$; Figure S3: Job plot for the binding of **NATB** with Al^{3+} (50 μM) in MeOH. Fluorescence intensity at 526 nm is plotted as a function of the molar ratio of $[\text{Al}^{3+}]/([\text{Al}^{3+}] + [\text{NATB}])$; Figure S4: Positive-ion ESI mass spectrum of **NATB** (100 μM) in MeOH upon the addition of 1 equiv of Al^{3+} in DMF; Figure S5: Li's equation plot (at 526 nm) of **NATB** (30 μM) in MeOH, based on fluorescence titration, assuming 1:1 stoichiometry for association between **NATB** and Al^{3+} ; Figure S6: Calibration curve of **NATB** as a function of Al^{3+} concentration in MeOH. $[\text{NATB}] = 30 \mu\text{M}$ and $[\text{Al}^{3+}] = 0\text{--}18 \mu\text{M}$ ($\lambda_{\text{ex}} = 358 \text{ nm}$); Figure S7: Competitive experiments of **NATB** (30 μM) toward Al^{3+} (45 μM) in the presence of other metal ions (45 μM , $\lambda_{\text{ex}} = 358 \text{ nm}$) in MeOH; Figure S8: (a) The theoretical excitation energies and the experimental UV-Vis spectrum of **NATB**. (b) The major electronic transition energies and molecular orbital contributions of **NATB**; Figure S9: (a) The theoretical excitation energies and the experimental UV-Vis spectrum of **NATB**- Al^{3+} . (b) The major electronic transition energies and molecular orbital contributions of **NATB**- Al^{3+} ; Figure S10: The major molecular orbital transitions and excitation energies of **NATB** and **NATB**- Al^{3+} ; Figure S11: UV-Vis spectra of **NATB** and **NATB**- Al^{3+} with H_2PO_4^- in MeOH, respectively; Figure S12: Job plot for the stoichiometry of **NATB**- Al^{3+} with H_2PO_4^- (30 μM) in MeOH. Fluorescence intensity at 526 nm is plotted as a function of the molar ratio of $[\text{NATB}-\text{Al}^{3+}]/([\text{NATB}-\text{Al}^{3+}] + [\text{H}_2\text{PO}_4^-])$; Figure S13: Positive-ion ESI mass spectrum of **NATB**- Al^{3+} (100 μM) in MeOH upon the addition of 1 equiv of H_2PO_4^- in H_2O ; Figure S14: Li's equation plot (at 526 nm) of **NATB**- Al^{3+} (30 μM) based on fluorescence titration in MeOH, assuming 1:1 stoichiometry for association between **NATB**- Al^{3+} and H_2PO_4^- ; Figure S15: Calibration curve of **NATB**- Al^{3+} in MeOH as a function of H_2PO_4^- concentration. $[\text{NATB}-\text{Al}^{3+}] = 30 \mu\text{M}$ and $[\text{H}_2\text{PO}_4^-] = 0.0\text{--}18.0 \mu\text{M}$ ($\lambda_{\text{ex}} = 358 \text{ nm}$); Figure S16: Interference studies of **NATB**- Al^{3+} (30 μM) toward H_2PO_4^- (45 μM) in the presence of other anions (45 μM , $\lambda_{\text{ex}} = 358 \text{ nm}$) in MeOH.

Author Contributions: D.C. and C.K. provided the initial idea for this work; D.C. contributed to the collection and analysis of field test data; D.C. and C.K. wrote the paper. All authors have read and agreed to the published version of the manuscript.

Funding: National Research Foundation of Korea (2018R1A2B6001686) is acknowledged.

Conflicts of Interest: The authors declare no conflict of interest.

References

1. Pungut, N.A.S.; Saad, H.M.; Sim, K.S.; Tan, K.W. A turn on fluorescent sensor for detecting Al^{3+} and colorimetric detection for Cu^{2+} : Synthesis, cytotoxicity and on-site assay kit. *J. Photochem. Photobiol. A Chem.* **2021**, *414*, 113290. [[CrossRef](#)]
2. Maity, D.; Govindaraju, T. Pyrrolidine constrained bipyridyl-dansyl click fluoroionophore as selective Al^{3+} sensor. *Chem. Commun.* **2010**, *46*, 4499–4501. [[CrossRef](#)]
3. Kim, S.Y.; Lee, S.Y.; Kang, J.H.; Kim, M.S.; Kim, A.; Kim, C. Colorimetric detection of $\text{Fe}^{3+/2+}$ and fluorescent detection of Al^{3+} in aqueous media: Applications and DFT calculations. *J. Coord. Chem.* **2018**, *71*, 2401–2414. [[CrossRef](#)]
4. Kaur, R.; Saini, S.; Kaur, N.; Singh, N.; Jang, D.O. Rhodamine-based fluorescent probe for sequential detection of Al^{3+} ions and adenosine monophosphate in water. *Spectrochim. Acta Part A Mol. Biomol. Spectrosc.* **2020**, *225*, 117523. [[CrossRef](#)]

5. Cheah, P.W.; Heng, M.P.; Izati, A.; Ng, C.H.; Tan, K.W. Rhodamine B conjugate for rapid colorimetric and fluorimetric detection of aluminium and tin ions and its application in aqueous media. *Inorg. Chim. Acta* **2020**, *512*, 119901. [[CrossRef](#)]
6. Maity, D.; Govindaraju, T. A differentially selective sensor with fluorescence turn-on response to Zn^{2+} and dual-mode ratiometric response to Al^{3+} in aqueous media. *Chem. Commun.* **2012**, *48*, 1039–1041. [[CrossRef](#)]
7. Zhou, J.; Yuan, Y.-F.; Zhuo, J.-B.; Lin, C.-X. Synthesis and characterization of cyclophane: The highly selective recognition of Fe^{3+} in aqueous solution and $H_2PO_4^-$ in acetonitrile solution. *Tetrahedron Lett.* **2018**, *59*, 1059–1064. [[CrossRef](#)]
8. Singh, A.; Nishith, U.; Trivedi, D.R. Spectroscopic studies of colorimetric receptors for detection of biologically important inorganic F^- , AcO^- and $H_2PO_4^-$ anions in organo-aqueous medium: Real-life application. *Inorg. Chem. Commun.* **2020**, *115*, 107874. [[CrossRef](#)]
9. Goswami, S.; Maity, S.; Maity, A.C.; Das, A.K.; Khanra, K.; Mandal, T.K.; Bhattacharyya, N. A macrocyclic piperazine linked extremely Zn^{2+} selective fluorescent chemosensor with bio-imaging and for $H_2PO_4^-$ sensing. *Tetrahedron Lett.* **2014**, *55*, 5993–5997. [[CrossRef](#)]
10. Cao, C.; You, X.; Feng, L.; Luo, G.; Yue, G.; Ji, X. Synthesis of new chromogenic sensors containing thiourea and selective detection for F^- , $H_2PO_4^-$, and Ac^- anions. *Can. J. Chem.* **2020**, *98*, 659–666. [[CrossRef](#)]
11. Choi, J.H.; Pandith, A.; Chakradhar, D.; Kim, H.R.; Kim, H.S. Al^{3+} -Morpholine-appended Anthracene Ensemble as a Dual Photonic Switch for $H_2PO_4^-$ and CN^- Ions and its Biological Applications. *Bull. Korean Chem. Soc.* **2019**, *40*, 138–145. [[CrossRef](#)]
12. Pandith, A.; Uddin, N.; Choi, C.H.; Kim, H.S. Highly selective imidazole-appended 9,10-*N,N'*-diaminomethylantracene fluorescent probe for switch-on Zn^{2+} detection and switch-off $H_2PO_4^-$ and CN^- detection in 80% aqueous DMSO, and applications to sequential logic gate operations. *Sens. Actuators B Chem.* **2017**, *247*, 840–849. [[CrossRef](#)]
13. Theetharappan, M.; Neelakantan, M.A. A Water-Soluble Schiff Base Turn-on Fluorescent Chemosensor for the Detection of Al^{3+} and Zn^{2+} Ions at the Nanomolar Level: Application in Live-Cell Imaging. *J. Fluoresc.* **2021**, *31*, 1277–1290. [[CrossRef](#)]
14. Chandra, R.; Manna, A.K.; Sahu, M.; Rout, K.; Patra, G.K. Simple salicylaldehyde-functionalized dipodal *bis* Schiff base chromogenic and fluorogenic chemosensors for selective and sensitive detection of Al^{3+} and Cr^{3+} . *Inorg. Chim. Acta* **2020**, *499*, 119192. [[CrossRef](#)]
15. Jeong, H.Y.; Lee, S.Y.; Han, J.; Lim, M.H.; Kim, C. Thiophene and diethylaminophenol-based “turn-on” fluorescence chemosensor for detection of Al^{3+} and F^- in a near-perfect aqueous solution. *Tetrahedron* **2017**, *73*, 2690–2697. [[CrossRef](#)]
16. Wang, M.; Lu, L.; Song, W.; Wang, X.; Sun, T.; Zhu, J.; Wang, J. AIE-active Schiff base compounds as fluorescent probe for the highly sensitive and selective detection of Al^{3+} ions. *J. Lumin.* **2021**, *233*, 117911. [[CrossRef](#)]
17. Park, S.M.; Saini, S.; Park, J.E.; Singh, N.; Jang, D.O. A benzothiazole-based receptor for colorimetric detection of Cu^{2+} and S^{2-} ions in aqueous media. *Tetrahedron Lett.* **2021**, *73*, 153115. [[CrossRef](#)]
18. So, H.; Cho, H.; Lee, H.; Tran, M.C.; Kim, K.T.; Kim, C. Detection of zinc (II) and hypochlorite by a thiourea-based chemosensor via two emission channels and its application in vivo. *Microchem. J.* **2020**, *155*, 104788. [[CrossRef](#)]
19. Feng, X.; Fu, Y.; Jin, J.; Wu, J. A highly selective and sensitive fluorescent sensor for relay recognition of Zn^{2+} and $HSO_4^-/H_2PO_4^-$ with “on-off” fluorescent responses. *Anal. Biochem.* **2018**, *563*, 20–24. [[CrossRef](#)]
20. Du, K.; Niu, S.; Qiao, L.; Dou, Y.; Zhu, Q.; Chen, X.; Zhang, P. A highly selective ratiometric fluorescent probe for the cascade detection of Zn^{2+} and $H_2PO_4^-$ and its application in living cell imaging. *RSC Adv.* **2017**, *7*, 40615–40620. [[CrossRef](#)]
21. Hwang, S.M.; Kim, M.S.; Lee, M.; Lim, M.H.; Kim, C. Single fluorescent chemosensor for multiple targets: Sequential detection of Al^{3+} and pyrophosphate and selective detection of F^- in near-perfect aqueous solution. *N. J. Chem.* **2017**, *41*, 15590–15600. [[CrossRef](#)]
22. Liu, Y.; Wang, X.; Feng, E.; Fan, C.; Pu, S. A highly selective sequential recognition probe for Zn^{2+} and $HSO_4^-/H_2PO_4^-$ based on a diarylethene chemosensor. *Spectrochim. Acta Part A Mol. Biomol. Spectrosc.* **2021**, *246*, 119052. [[CrossRef](#)] [[PubMed](#)]
23. Jain, H.; Deswal, N.; Joshi, A.; Ramachandran, C.N.; Kumar, R. Triazole-appended pyrano[2,3-*c*]pyrazolone based colorimetric chemosensors for recognition of Fe^{3+} ions and their molecular logic gate behavior. *Anal. Methods* **2019**, *11*, 3230–3243. [[CrossRef](#)]
24. Qu, W.J.; Yan, G.T.; Ma, X.L.; Wei, T.B.; Lin, Q.; Yao, H.; Zhang, Y.M. “Cascade recognition” of Cu^{2+} and $H_2PO_4^-$ with high sensitivity and selectivity in aqueous media based on the effect of ESIPT. *Sens. Actuators B Chem.* **2017**, *242*, 849–856. [[CrossRef](#)]
25. Li, S.; Cao, D.; Meng, X.; Hu, Z.; Li, Z.; Yuan, C.; Zhou, T.; Han, X.; Ma, W. A novel schiff base fluorescent probe based on coumarin and benzothiazole for sequential detection of Al^{3+} and PPi and its applicability in live cell imaging. *J. Photochem. Photobiol. A Chem.* **2020**, *392*, 112427. [[CrossRef](#)]
26. Fu, J.; Li, B.; Mei, H.; Chang, Y.; Xu, K. Fluorescent schiff base probes for sequential detection of Al^{3+} and F^- and cell imaging applications. *Spectrochim. Acta Part A Mol. Biomol. Spectrosc.* **2020**, *227*, 117678. [[CrossRef](#)] [[PubMed](#)]
27. Sun, X.J.; Liu, T.T.; Fu, H.; Li, N.N.; Xing, Z.Y.; Yang, F. A Naphthalimide-Based Fluorescence “Off-on-Off” Chemosensor for Relay Detection of Al^{3+} and ClO^- . *Front. Chem.* **2019**, *7*, 549. [[CrossRef](#)]
28. Huang, M.X.; Lai, J.P.; Sun, H.; Wu, W.Z. A simple, highly selective and ultra-sensitive “off-on-off” fluorescent chemosensor for successive detection of aluminum ion and phosphate in water samples. *Microchem. J.* **2019**, *151*, 104195. [[CrossRef](#)]
29. Zhang, Y.M.; Chen, X.P.; Liang, G.Y.; Zhong, K.P.; Yao, H.; Wei, T.B.; Lin, Q. A water-soluble fluorescent chemosensor based on Asp functionalized naphthalimide for successive detection Fe^{3+} and $H_2PO_4^-$. *Can. J. Chem.* **2018**, *96*, 363–370. [[CrossRef](#)]
30. Meng, X.; Li, S.; Ma, W.; Wang, J.; Hu, Z.; Cao, D. Highly sensitive and selective chemosensor for Cu^{2+} and $H_2PO_4^-$ based on coumarin fluorophore. *Dyes Pigments* **2018**, *154*, 194–198. [[CrossRef](#)]

31. Purkait, R.; Das Mahapatra, A.; Chattopadhyay, D.; Sinha, C. An azine-based carbothioamide chemosensor for selective and sensitive turn-on-off sequential detection of Zn(II) and H_2PO_4^- , live cell imaging and INHIBIT logic gate. *Spectrochim. Acta Part A Mol. Biomol. Spectrosc.* **2019**, *207*, 164–172. [[CrossRef](#)] [[PubMed](#)]
32. Kumar, A.; Kumar, V.; Upadhyay, K.K. An Al^{3+} and $\text{H}_2\text{PO}_4^-/\text{HSO}_4^-$ selective conformational arrest and bail to a pyrimidine-naphthalene anchored molecular switch. *Analyst* **2013**, *138*, 1891–1897. [[CrossRef](#)] [[PubMed](#)]
33. Anu, D.; Naveenm, P.; Rajamanikandan, R.; Kaveri, M.V. Development of hydrazide based fluorescence probe for detection of Al^{3+} ions and application in live cell image. *J. Photochem. Photobiol. A Chem.* **2021**, *405*, 112921. [[CrossRef](#)]
34. Sun, J.; Li, Y.; Shen, S.; Yan, Q.; Xia, G.; Wang, H. A squaraine-based fluorescence turn on chemosensor with ICT character for highly selective and sensitive detection of Al^{3+} in aqueous media and its application in living cell imaging. *Spectrochim. Acta Part A Mol. Biomol. Spectrosc.* **2020**, *228*, 117590. [[CrossRef](#)]
35. Xu, Y.; Kong, L.; Bai, L.; Chen, A.; Li, N.; Cheng, L.; Liu, W.; Sun, X.; Tao, F.; Wang, L.; et al. A new water-soluble polymer fluorescent chemosensor with thiophene Schiff base site for selectively sensing Al^{3+} ions. *Tetrahedron* **2021**, *79*, 131888. [[CrossRef](#)]
36. Li, Z.; Wang, Q.; Wang, J.; Jing, X.; Wang, S.; Xiao, L.; Li, L. A fluorescent light-up probe for selective detection of Al^{3+} and its application in living cell imaging. *Inorg. Chim. Acta* **2020**, *500*, 119231. [[CrossRef](#)]
37. Liao, Z.; Liu, Y.; Han, S.F.; Wang, D.; Zheng, J.Q.; Zheng, X.J.; Jin, L.P. A novel acylhydrazone-based derivative as dual-mode chemosensor for Al^{3+} , Zn^{2+} and Fe^{3+} and its applications in cell imaging. *Sens. Actuators B Chem.* **2017**, *244*, 914–921. [[CrossRef](#)]
38. Zhu, G.; Huang, Y.; Wang, C.; Lu, L.; Sun, T.; Wang, M.; Tang, Y.; Shan, D.; Wen, S.; Zhu, J. A novel coumarin-based fluorescence chemosensor for Al^{3+} and its application in cell imaging. *Spectrochim. Acta Part A Mol. Biomol. Spectrosc.* **2019**, *210*, 105–110. [[CrossRef](#)]
39. Das, A.K.; Goswami, S. 2-Hydroxy-1-naphthaldehyde: A versatile building block for the development of sensors in supramolecular chemistry and molecular recognition. *Sens. Actuators B Chem.* **2017**, *245*, 1062–1125. [[CrossRef](#)]
40. Immanuel David, C.; Bhuvanesh, N.; Jayaraj, H.; Thamilselvan, A.; Parimala Devi, D.; Abiram, A.; Prabhu, J.; Nandhakumar, R. Experimental and Theoretical Studies on a Simple S-S-Bridged Dimeric Schiff Base: Selective Chromo-Fluorogenic Chemosensor for Nanomolar Detection of Fe^{2+} & Al^{3+} Ions and Its Varied Applications. *ACS Omega* **2020**, *5*, 3055–3072. [[CrossRef](#)]
41. Das, B.; Dolai, M.; Dhara, A.; Ghosh, A.; Mabhaj, S.; Misra, A.; Dey, S.; Jana, A. Solvent-Regulated Fluorimetric Differentiation of Al^{3+} and Zn^{2+} Using an AIE-Active Single Sensor. *J. Phys. Chem. A* **2021**, *125*, 1490–1504. [[CrossRef](#)]
42. Singh, R.; Das, G. “Turn-on” Pb^{2+} sensing and rapid detection of biothiols in aqueous medium and real samples. *Analyst* **2019**, *144*, 567–572. [[CrossRef](#)]
43. Yang, R.; Li, K.; Wang, K.; Zhao, F.; Li, N.; Liu, F. Porphyrin assembly on β -cyclodextrin for selective sensing and detection of a zinc ion based on the dual emission fluorescence ratio. *Anal. Chem.* **2003**, *75*, 612–621. [[CrossRef](#)] [[PubMed](#)]
44. Frisch, M.J.; Trucks, G.W.; Schlegel, H.B.; Scuseria, G.E.; Robb, M.A.; Cheeseman, J.R.; Scalmani, G.; Barone, V.; Petersson, G.A.; Nakatsuji, H.; et al. *Gaussian 16, Revision C.01*; Gaussian, Inc.: Wallingford, CT, USA, 2016.
45. Becke, A.D. Density-functional thermochemistry. III. The role of exact exchange. *J. Chem. Phys.* **1993**, *98*, 5648–5652. [[CrossRef](#)]
46. Lee, C.; Yang, W.; Parr, R.G. Development of the Colle-Salvetti correlation-energy formula into a functional of the electron density. *Phys. Rev. B* **1988**, *37*, 785–789. [[CrossRef](#)] [[PubMed](#)]
47. Hariharan, P.C.; Pople, J.A. The influence of polarization functions on molecular orbital hydrogenation energies. *Theor. Chim. Acta* **1973**, *28*, 213–222. [[CrossRef](#)]
48. Francl, M.M.; Pietro, W.J.; Hehre, W.J.; Binkley, J.S.; Gordon, M.S.; DeFrees, D.J.; Pople, J.A. Self-consistent molecular orbital methods. XXIII. A polarization-type basis set for second-row elements. *J. Chem. Phys.* **1982**, *77*, 3654–3665. [[CrossRef](#)]
49. Hay, P.J.; Wadt, W.R. Ab initio effective core potentials for molecular calculations. Potentials for the transition metal atoms Sc to Hg. *J. Chem. Phys.* **1985**, *82*, 270–283. [[CrossRef](#)]
50. Wadt, W.R.; Hay, P.J. Ab initio effective core potentials for molecular calculations. Potentials for main group elements Na to Bi. *J. Chem. Phys.* **1985**, *82*, 284–298. [[CrossRef](#)]
51. Hay, P.J.; Wadt, W.R. Ab initio effective core potentials for molecular calculations. Potentials for K to Au including the outermost core orbitals. *J. Chem. Phys.* **1985**, *82*, 299–310. [[CrossRef](#)]
52. Klamt, A.; Moya, C.; Palomar, J. A Comprehensive Comparison of the IEFPCM and SS(V)PE Continuum Solvation Methods with the COSMO Approach. *J. Chem. Theory Comput.* **2015**, *11*, 4220–4225. [[CrossRef](#)] [[PubMed](#)]
53. Jo, T.G.; Bok, K.H.; Han, J.; Lim, M.H.; Kim, C. Colorimetric detection of Fe^{3+} and Fe^{2+} and sequential fluorescent detection of Al^{3+} and pyrophosphate by an imidazole-based chemosensor in a near-perfect aqueous solution. *Dyes Pigments* **2017**, *139*, 136–147. [[CrossRef](#)]